NWP SAF

Satellite Application Facility
for Numerical Weather Prediction

Document No. NWPSAF–EC–TR–008

Version 1.0

July 2003

The capability of 4D-Var systems to assimilate cloud-affected satellite infrared radiances

F. Chevallier, P. Lopez,

A. M. Tompkins, M. Janisková and E. Moreau

European Centre for Medium–Range Weather Forecasts

Submitted for publication in Q. J. Roy. Meteor. Soc.

The capability of 4D-Var systems to assimilate cloud-affected satellite infrared radiances

F. Chevallier, P. Lopez, A. M. Tompkins, M. Janisková and E. Moreau

ECMWF

This documentation was developed within the context of the EUMETSAT satellite Application Facility on Numerical Weather Prediction (NWP SAF), under the Cooperation Agreement dated 25 November 1998, between EUMETSAT and the Met Office, UK, by one or more partners within the NWP SAF. The partners in the NWP SAF are the Met Office, ECMWF, KNMI and Météo France.

Change record			
Version	Date	Author / changed by	Remarks

Abstract

Four-dimensional variational (4D-Var) assimilation schemes assume the linearity of their forward model in the vicinity of prior information and consequently do not properly handle variables that have fine temporal and spatial scales compared to the forward model. Hence cloud-affected satellite infrared radiances are discarded from numerical weather prediction 4D-Var systems despite the critical need of observations within the cloudy regions. This paper suggests the reappraisal of that choice, subject to achieving improvements in the modelling of clouds.

A new observation operator, that computes cloud-affected infrared radiances from 4D-Var control variables, namely atmospheric temperature, humidity, ozone, surface temperature and surface pressure, is presented. The vertical distributions of cloud cover and of cloud condensate are diagnosed in the operator itself. The goal of this paper is to assess the feasibility of using it to assimilate cloud-affected infrared radiances such as those from the narrow-band Advanced Infrared Sounder on-board the Aqua platform or those from the broad-band Meteosat Visible and Infrared Instrument. It is shown that there is a potential benefit in assimilating some of the upper tropospheric channels at 4.5, 6.3 and 14.3 μm in the presence of clouds directly in 4D-Var, for instance the 6.3 μm channel on-board all the geostationary satellites.

1 Introduction

The improvement of weather forecast skill in recent years owes much to the development of Bayesian estimation techniques for atmospheric data assimilation. In particular, an increasing number of numerical weather prediction (NWP) centres opt for three- and four-dimensional variational assimilation systems (respectively 3D-Var and 4D-Var) to perform their atmospheric analyses (e.g. Rabier et al. 2000, Lorenc et al. 2000). 3D- and 4D-Var estimate the atmospheric variables from a background state (usually based on an earlier forecast) and from available observations. They perform best when background and observation error statistics are Gaussian, unbiased and perfectly known, and when the forward model, that relates the background variables to the observed variables, is linear. Linearity is actually only needed in the vicinity of the background for perturbations whose magnitude is of the same order as the background errors. Yet observations for which significant non-linearities affect the forward model are discarded from 3D- and 4D-Var systems. Consequently, infrared satellite radiances are currently not assimilated in the presence of clouds, even though they would inform the NWP systems about critical regions of the atmosphere (McNally 2002).

At European Centre for Medium-Range Weather Forecasts (ECMWF) an observation operator that computes cloud-affected radiances from some of the ECMWF 4D-Var control variables (temperature, humidity and ozone profiles, surface temperature and surface pressure) has been developed for data assimilation. The operator diagnoses the vertical distributions of cloud cover and of cloud condensate by taking both large-scale and convective processes into consideration. The goal of this paper is to assess the possibility of its use for assimilating cloud-affected radiances within a 4D-Var system. The assessment is based on the examination of the accuracy and

of the linearity of this new observation operator for the simulation of the narrow-band channels from Advanced Infrared Sounder (AIRS) on-board the Aqua platform and of the broad-band channels from the Meteosat Visible and Infrared Instrument (MVIRI).

The plan of the paper is as follows. Section 2 outlines the 4D-Var method and discusses the implications for the selection of observations. Section 3 describes the data and the observation operator. Accuracy and linearity of the observation operator are estimated in sections 4 and 5 respectively. Concluding discussion follows in section 6.

2 Theoretical framework of 4D-Var

2.1 General formalism

4D-Var systems are a practical formulation of Bayesian estimation theory for the particular case of a linear problem with un-biased Gaussian errors. They seek a model trajectory $\mathbf{x}(t)$ that is statistically consistent with the information provided by the observations $\mathbf{y}$ available during a given time period $[t_0,\, t_n]$ and that provided by an *a priori* model state $\mathbf{x}^b$ called the background state. The background $\mathbf{x}^b$ is usually based on a short-range forecast. The model trajectory $\mathbf{x}(t)$ is completely defined by the initial state $\mathbf{x}_0$ at time t_0.

The balance of the model initial state $\mathbf{x}_0$ between the observations $\mathbf{y}$ and the background $\mathbf{x}^b$ is measured by an objective cost-function defined as follows:

$$J(\mathbf{x}_0) = \frac{1}{2}(\mathbf{x}_0 - \mathbf{x}_0^b)^T \mathbf{B}^{-1}(\mathbf{x}_0 - \mathbf{x}_0^b) + \frac{1}{2}\sum_i (\psi_i[\mathbf{x}_0] - \mathbf{y}_i)^T \mathbf{R}_i^{-1}(\psi_i[\mathbf{x}_0] - \mathbf{y}_i) \qquad (1)$$

where at any time t_i, $\mathbf{y}_i$ is the vector of observations, ψ_i is the forward operator providing the equivalent of the observations from the model initial state $\mathbf{x}_0$, $\mathbf{R}_i$ is the observation error covariance matrix and $\mathbf{B}$ is the background error covariance matrix of the state $\mathbf{x}^b$. Superscripts -1 and T denote respectively inverse and transpose matrix. Subscript i denotes the time index.

ψ_i is the combination of a dynamic *model operator*, usually called M_i, and of a static *observation operator*, usually called H_i (Ide et al. 1997). Observation errors described by $\mathbf{R}_i$ are assumed to be uncorrelated from one time step i to another. It is important to understand that they are defined with respect to the forward model ψ_i which is assumed to be perfect. Consequently, $\mathbf{R}_i$ actually contains the errors of ψ_i in addition to the measurement errors.

The control vector $\mathbf{x}_0$ includes the prognostic variables to be initialized in the forecast model: vorticity, divergence, temperature, humidity, ozone, surface temperature and surface pressure in the case of the ECMWF 4D-Var. Surface temperature is actually defined at satellite observation points only since soil variables are specifically analysed in a separate Optimal Interpolation system. In theory, cloud cover and cloud condensate could be 4D-Var control variables as well, but the definition of their background errors and of their coupling with temperature and humidity background errors would be particularly challenging, for instance when cloud cover is zero or unity.

The minimization uses a descent algorithm which requires several computations of the gradient of J with respect to the initial state $\mathbf{x}_0$. Given the dimension of the state vector the adjoint technique is used to provide an efficient estimate of ∇J:

$$\nabla J(\mathbf{x}_0) = \mathbf{B}^{-1}(\mathbf{x}_0 - \mathbf{x}_0^b) + \sum_i \mathbf{\Psi}_i^T \mathbf{R}_i^{-1}(\psi_i[\mathbf{x_0}] - \mathbf{y}_i) \tag{2}$$

where $\mathbf{\Psi}_i^T$ is the adjoint of the forward operator (i.e. the derivative or Jacobian matrix).

Additionally, an incremental formulation of the variational system is used at ECMWF (Courtier et al. 1994): departures $\psi_i[\mathbf{x}_0] - \mathbf{y}_i$ are computed at resolution 40 km, the analysis increments are computed at the lower resolution of 125 km. The system copes with weak non-linearities through an "inner-loop/outer-loop algorithm", where the cost function is minimised in the the inner loop based on a linearisation of ψ_i in the vicinity of the initial state which is updated in the outer loop. A simplified version of the derivatives of ψ_i are used both for the linearisation (tangent-linear model $\mathbf{\Psi}_i$) and for the adjoint model $\mathbf{\Psi}_i^T$. In the following, cycle 25r5 of the ECMWF forecasting system that became operational in March 2003 is used.

2.2 Implications for the selection of cloud-affected observations

The variational formulation of the inverse problem outlined above, together with currently available computer power allows the operational handling of large numbers of control variables (about 5 million currently at ECMWF) and of observations (about 1.5 million per 12-hour analysis cycle). It would provide statistically optimal analyses if the errors statistics $\mathbf{B}$ and $\mathbf{R}_i$ were un-biased, Gaussian and perfectly known and if the problem was linear. For instance significant non-linearities may exist in a 4D-Var system, but they degrade the realism of the corresponding analyses and tend to limit the impact in the subsequent forecasts to short ranges. As a consequence, attempts are made to bring the 4D-Var systems as close as possible to optimality by removal of biases (e.g. Harris and Kelly 2001), by choosing Gaussian error control variables (e.g. Dee and da Silva 2003), by a careful estimation of the error statistics (e.g. Derber and Bouttier 1999), by the improvement of the parameterizations of the forward operator and by avoiding observations for which ψ_i is significantly non-linear with respect to the analysis increments $\mathbf{x}_0 - \mathbf{x}_0^b$.

To account for cloud processes in such a framework is obviously a challenge. Indeed, fine-scale atmospheric processes significantly impact the cloud fields and result in significant non-linearities at the spatial and temporal scales of the NWP models. Further, they make cloud parameterizations particularly difficult to formulate. Conversely, cloud observations also contain large-scale information, through the dynamics, which allows a realistic representation of cloud systems in NWP (e.g. Chevallier and Kelly 2002). In the next sections the accuracy of the recently-developed observation operator and its linearity with respect to perturbations of the order of the expected size of analysis increments will be estimated in order to select cloud-affected channels for assimilation within 4D-Var.

3 Data and model

3.1 The satellite data

The present study exploits the observations from two space-borne instruments, MVIRI and AIRS.

MVIRI has been flown on-board the Meteosat 1 to 7 geostationary satellites, operated by the European Organisation for the Exploitation of Meteorological Satellites (EUMETSAT). It includes three spectrally-broad measurement channels: two infrared ones (from 10.5 to 12.5 μm and from 5.7 to 7.1 μm respectively) and one visible (0.45 to 1 μm). An image of the earth disc as seen by the geostationary orbit is generated at 30 minute intervals in each channel. It consists of 2500×2500 pixels for the infrared channels (5×5 km^2 resolution at the subsatellite point) and 5000×5000 pixels (2.5×2.5 km^2) for the visible one. One Meteosat satellite is normally stationed above Africa, but depending on operational choice, an additional one may be positioned above the Atlantic or the Indian Ocean.

For the present study, the radiances from the two infrared Meteosat channels are extracted from the EUMETSAT Radiance Data from Clouds (RDC) product in the form of mean brightness temperatures in 16×16 pixel quadrants. This averaging results in a resolution (80 km at the subsatellite point) similar to the ECMWF analysis (currently about 125 km). It is useful to note that data from a connected EUMETSAT product, the Clear Sky Radiances (CSR), are operationally assimilated at ECMWF (Munro et al. 1999). Those radiances result from averages for the pixels not affected by clouds in each quadrant. Only data from the quadrants where more than 70% of the pixels are judged clear are actually assimilated. Consistently, quadrants will be considered cloudy in the following when more than 30% of the pixels are not classified as clear.

The AIRS instrument, operated by the National Aeronautic and Space Agency (NASA), provides significantly different measurements of the infrared spectrum. On-board the Aqua sun-synchronous polar orbiter, it observes nearly all points of the globe twice a day, moving northward across the equator at about 01:30 PM local time. It samples the infrared spectrum between 3.7 and 15.4 μm with 2378 channels. Additionally 4 channels are located in the visible (from 0.4 to 1.0 μm). Horizontal resolution reaches 13.5 km and 2.3 km at nadir for the infrared and the visible channels respectively. No attempt is made to average the data. As a starting point, a subset of 324 channels for one satellite spot in eighteen has been made operationally available to ECMWF by the National Environment Satellite Data and Information Service (NESDIS). Data from cloud-free channels are currently assimilated in a research mode, with a cloud detection method described by McNally and Watts (2003).

AIRS observations for wave numbers below 2000 cm^{-1} and MVRI ones are bias-corrected using a constant offset in each channel in order to account for possible erroneous knowledge of the instrument characteristics. The offset is estimated independently from cloud-free departure statistics (Köpken and McNally 2003, personal communication).

3.2 Observation operator

3.2.1 Diagnostic and prognostic models

A prognostic model implies a scheme that computes the tendencies $\partial\eta/\partial t$ of some cloud quantity η with respect to time t, therefore retaining cloud information from previous time-steps of the integration. A diagnostic model alternatively diagnoses the state of η at time t from other variables, thus precluding a memory of cloud variables and thus implying that cloud mass is not necessarily conserved.

The ECMWF forecast model includes a prognostic cloud scheme (Tiedtke 1989, 1993) which could in principle be used in the 4D-Var physics for the assimilation of cloud information, provided that cloud variables are added in the 4D-Var control vector. Such a strategy would pose the acute problem of defining background error statistics for the new variables, as mentioned in section 2.1. As a consequence, a diagnostic approach has been preferred. A model has been developed and is described hereafter. It uses only the existing 4D-Var control variables as input and was kept relatively simple so that thresholds and strong non-linearities do not make the 4D-Var minimization stop before reaching the absolute minimum of the cost function.

The present study does not cover the full 4D-Var forward model. It focuses mainly on its static part, or observation operator H (see section 2.1), that computes satellite radiances from the relevant 4D-Var control variables, namely atmospheric temperature, humidity, ozone, surface temperature and surface pressure. Indeed the dynamic part, or model operator M, computes the time evolution of all the control variables and is not specific to the assimilation of radiances in the presence of clouds. The reader is referred to Janisková et al. (2002) for the impact of the introduction of cloud-radiation interaction within the model operator.

3.2.2 Convection model

The convection model of the observation operator is based on the ECMWF operational mass-flux scheme, initiated by Tiedtke (1989), but uses a simplified algorithm. All types of convection (shallow, mid-level, and deep) are treated in a similar way. In particular, the link between the model control variables and the subgrid-scale convective quantities (the so-called closure assumption) is expressed through a single formulation that depends on the release of convective available potential energy in time. The equations that describe the vertical evolution of the updraught mass-flux M_u and of the updraught thermodynamic variables Φ_u are uncoupled:

$$\frac{\partial M_u}{\partial z} = -(\epsilon - \delta) M_u \tag{3}$$

$$\frac{\partial \Phi_u}{\partial z} = -\epsilon(\Phi_u - \overline{\Phi}) \tag{4}$$

where $\overline{\Phi}$ denotes field values in the environment, and ϵ and δ are the entrainment and detrainment fractional rates respectively. The bulk convective updraught is assumed to originate

from the surface only if its initial vertical velocity as calculated from the surface heat fluxes is positive. The departures of the updraught from the environment are also assumed to be dependent on the surface heat fluxes. If convection cannot be initiated from the surface, the convective ascent may originate from higher levels provided relative humidity exceeds 80%. In this case, the initial vertical velocity of the bulk updraught is set equal to 1 m s^{-1}. Regardless of whether the updraught originates from the surface or higher up, the vertical evolution of its kinetic energy is computed following Simpson and Wiggert (1969) which involves the entrainment of environmental air into the updraught. Convection is assumed to be active only if the updraught vertical velocity remains positive at cloud base. Simplified calculations of downdraughts and convective momentum transport, based on the operational scheme, are also included in the modified parameterization. The calculation of the precipitation formation rate from the updraught cloud condensate specific content is inspired from Tiedtke (1989). Further details of the convection scheme are given by Moreau et al. (2003).

3.2.3 Large-scale cloud model

As described by Tompkins and Janisková (2003), the stratiform part of the diagnostic cloud scheme assumes that the subgrid-scale fluctuations of total water are uniformly distributed. Two parameters only are therefore needed to describe the corresponding probability density function (PDF) in any model layer i, hereafter RH_i^c and κ_i. RH_i^c is the critical relative humidity above which clouds are allowed to form, κ_i sets the total water variance, or equivalently the distribution width. Stratiform cloud cover in layer i is consequently expressed as:

$$C_i^{strat} = 1 - \sqrt{\frac{1 - RH_i}{1 - RH_i^c - \kappa_i(RH_i - RH_i^c)}}. \tag{5}$$

where RH_i is the relative humidity in layer i. RH_i^c and κ_i are empirically defined in each layer. Initially the RH_i^cs were estimated using $\kappa_i = 0.7$ so that the diagnostic model fits the prognostic scheme (Tiedtke 1993) well. Values of RH_i^c between 0.55 in the middle troposphere up to about 0.9 at the tropopause and at the surface were obtained. The coefficients κ_i were then adjusted to agree with top-of-the-atmosphere radiation observations. In addition, precipitation fluxes are estimated in a manner close to the prognostic scheme, in order to pave the way for the assimilation of rain-affected microwave radiances, but this aspect is not exploited here.

3.2.4 The radiation model

The radiation model has already been documented within previous studies (Chevallier et al. 2001, Chevallier and Kelly 2002, Chevallier et al. 2002) and only its salient features are recalled here. The scheme applies in the infrared as in the microwave spectrum, but does not take scattering into account. Cloud absorption is computed in each model layer using parameterizations similar to those used in the ECMWF forecast model for the broad-band radiative fluxes. Cloud layers are assumed to overlap according to the maximum-random scheme

of Raïsänen (1998). The Radiative Transfer for Television and Infrared Observation Satellite (TIROS) Operational Vertical Sounder (RTTOV: Eyre 1991, Saunders et al 2002) computes the gaseous absorption. The model has been used since 2000 for the routine monitoring of the clouds modelled by the ECMWF forecasting system in operations and in the 40-year re-analysis program.

4 Accuracy of the observation operator

4.1 MVIRI

The accuracy of the observation operator is illustrated for the Meteosat-7 data from 30 November 2002 at 12 UTC. The atmospheric circulation is very similar to that described in Chevallier and Kelly (2002) for December 2000. Various cloud systems are present in the 11 μm full resolution image (Figure 1): several frontal systems spread in the mid-latitudes and tropical convection is very active over the oceans as over land. Inputs to the observation operator are extracted from the 12-hour forecast initialized from the 00 UTC analysis. Cloud variables are diagnosed by the moist physics described above but can also be simply extracted from the forecast archive. In the latter case, the cloud variables are computed by the prognostic cloud scheme. The same radiation model is used in both cases. Although the forecast resolution reaches 40 km, a reduced grid of 80 km is used here for better compatibility with the 4D-Var system.

Statistics of the model vs. the observations are presented in Table 1 for the two infrared channels in the Meteosat cloudy quadrants. From this simple test, the diagnostic and the prognostic physics appear to perform similarly with respect to observations, despite significant standard deviations (9.6 K at 11 μm) of the differences between each other. This result is particularly important for 4D-Var applications, where the diagnostic model would be used in place of the prognostic one (see section 3.2.1). The largest departures from the observations occur around 11 μm. Indeed in this atmospheric spectral window little gaseous absorption takes place so that any cloud above the boundary layer has a strong impact on this channel. Comparatively, the 6.3 μm channel is very sensitive to upper tropospheric humidity (e.g. Schmetz and Turpeinen 1988). It is therefore hardly affected by low level clouds and less affected by upper- and mid-level clouds. The fraction of observed variance explained by the model is defined as $f = (Var[y] - Var[H[x] - y])/Var[y]$, where $Var[y]$ is the variance of the observation and $Var[H[x] - y]$ is the variance of the departures ($f = 1$ if the model is perfect and $f = 0$ if the model does not correlate with the observations). This fraction f is 0.48 and 0.20 respectively at 6.3 and 11 μm for the prognostic model and 0.46 and 0.04 respectively for the diagnostic model. This means that both models have some similar significant skill in predicting 80 km-resolution 6.3 μm cloud optical thickness, but have nearly none at 11 μm, at least on an average in the Meteosat disk. The deficiencies at 11 μm can be caused by the cloud scheme, the radiation model or by the temperature and humidity fields. One may note that the prognostic scheme is used in dynamic mode and is combined with other parameterizations in the forecast model to

predict the temperature and humidity variations.

It would be interesting to investigate the PDF of the observation operator errors, because they would dominate the observation error covariances $\mathbf{R}$ (time index i has been dropped and model operator is ignored) and would consequently be assumed to be Gaussian within 4D-Var (see section 2.1). Two methods could be used to infer $\mathbf{R}$. The first one would directly measure it with accurate validation data, including both the inputs and the outputs of the observation operator. Such data, for instance from the Atmospheric Radiation Measurement program (ARM, Stokes and Schwartz 1994), do not exist in sufficient number to build reliable error statistics. The second method would infer $\mathbf{R}$ indirectly from the PDF of the departures of the model from the observations, that include both observation and background errors, and from accurate estimation of the background error statistics $\mathbf{B}$. Rough estimates of $\mathbf{B}$ exist and are used below, but do not reach a sufficient accuracy for this task. Therefore the PDF of the departures in the cloudy quadrants is used here as a poor surrogate. They are shown in Figure 2 for the cloudy quadrants, together with the Gaussian distributions that have the same mean and standard deviation. There is no indication in the figure that the assumption of Gaussian shape for the observation errors is a significant issue in comparison to the accuracy and to the linearity properties.

4.2 AIRS

The model evaluation for the 324 available AIRS channels is less straightforward than for Meteosat because the AIRS spectrometer provides only few observations for a specific time. Model fields from several time steps are needed in order to accumulate a significant amount of collocated data. As a consequence, AIRS data are being passively monitored in the forecasting system (with ranges from 3 to 15 hours and at resolution 40 km), which takes the model data at observation time. Figure 3 presents the corresponding global statistics of the differences between the prognostic model and the observation for the cloud-affected AIRS channels on 30 November 2002. Other periods have been investigated and very similar results to those from Figure 3 have been obtained. For comparison, the wave-numbers covered by the MVIRI infrared filter functions are indicated in the legend of the figure. In addition Figure 4 displays the fraction of the cloud-affected observed variance explained by the model.

For technical reasons, the diagnostic model cannot be used yet for passive monitoring in the forecasting system. As a consequence, diagnostic and prognostic brightness temperature are compared independently to the real AIRS data, using the Meteosat-7 6.3 μm cloud mask for 30 November 2002 at 12 UTC. For each cloud-affected quadrant, equivalent AIRS brightness temperatures are computed using the diagnostic and the prognostic scheme. The zenith angle was set to that of Meteosat-7. Corresponding statistics are presented in Figure 5.

From Figure 3, it is obvious that the model statistics are the best in the channels least affected by clouds. Biases are mainly positive, showing that the model underestimates the cloud radiative forcing, consistent with the Meteosat validation and with previous studies (e.g. Chevallier et al. 2001). A different behaviour occurs for the near-infrared channels above

2500 cm^{-1}. Although they are window channels, the bias reduces with increasing wavenumber and finally changes sign. This is likely caused by the absence of cloud scattering and/or of cloud reflection in the radiation model. Large negative values occur around 2300 cm^{-1} for cloud-affected and for clear channels (McNally 2003, personal communication) and are being investigated. The fraction of variance explained by the model is much higher than for the Meteosat comparison (mentioned in Section 4.1) despite the discrepancy between the observation and the model resolutions (respectively 13 km at nadir and 40 km), which did not happen with Meteosat RDC. This apparent contradiction actually reflects the different orbits of the two instruments. Indeed mid-latitudes are better modelled than the Tropics, in particular over land, which favours the AIRS-based statistics. For instance, if the latitudes within 30° of the Equator are removed from the Meteosat statistics, the fraction of variance explained by the prognostic model reaches 0.66 and 0.89 at 6.3 and 11 μm respectively.

Since the diagnostic model has been tuned to radiation observations, the biases between diagnostic and prognostic brightness temperatures nearly cancel the biases between prognostic ones and observations (Figure 5). Standard deviations are slightly smaller between the two models than with observations, but are here much smaller than the observation "random" variations (not shown).

5 Linearity of the observation operator

The linearity assumption is tested here for perturbations $\delta\mathbf{x} = \mathbf{x} - \mathbf{x}^b$, that are of the order of magnitude expected in 4D-Var, i.e. comparable to the background errors. Consequently, the perturbations are defined based on the principal components of the ECMWF operational background error matrix $\mathbf{B}$ (Rabier et al. 1998, Derber and Bouttier 1999). Temperature errors vary with latitude and humidity error statistics are a function of relative humidity. Temperature and humidity errors are un-coupled. One $\delta\mathbf{x}$ is then a Gaussian perturbation applied to all principal components at once. This ensures that $\mathbf{B}$ is the covariance matrix of the perturbations.

The choice is made here to use the atmospheric profiles within the Meteosat-7 disk on 30 November 2002 at 12 UTC as a dataset sampling very diverse atmospheric conditions. For each cloud-affected quadrant, the correlation between the tangent-linear perturbations $\mathbf{H}\delta\mathbf{x}$ (where $\mathbf{H}$ is the adjoint of the observation operator) to the AIRS brightness temperatures and the non-linear ones $H[\mathbf{x}^b + \delta\mathbf{x}] - H[\mathbf{x}^b]$ is computed using an ensemble of 100 perturbations. The zenith angle is set to that of Meteosat-7. The PDF of the correlations is shown for each channel in Figure 6a. Stratospheric channels are easily identified because they correspond to the narrow PDFs close to unity, around wave-numbers 500 cm^{-1} and 2300 cm^{-1}. Channels that both have a sensitivity in the troposphere and systematically correspond to high correlations (e.g. above 0.85) can be found in the H_2O ν_2 band (around 1500 cm^{-1}) and next to the stratospheric channels (in the lower-wavenumber part of the CO_2 ν_2 band -around 700 cm^{-1}- and around 2250 cm^{-1}) only. Those few channels sound the upper troposphere only and are less affected by clouds. Channels with sensitivities lower down in the troposphere show high non-linear

behaviours. Reducing the humidity perturbations by a factor of two only slightly increases the correlations, as is shown in Figure 6b. This indicates that improvements in the quality of the background in the forthcoming years are not likely to change the status of those channels with respect to linearity. Results for MVIRI, with high correlations at 6.3 μm and low at 11 μm, do not bring additional information and are not reported here.

6 Conclusion

An observation operator has been developed, that computes cloud-affected satellite brightness temperatures from some of the ECMWF 4D-Var control variables: temperature, humidity and ozone profiles, surface temperature and surface pressure. It comprises a diagnostic cloud scheme with a representation of large-scale and convective processes and a radiation model. In order to evaluate the capability of 4D-Var systems to handle satellite infrared observations in the presence of clouds, its accuracy and its linearity have been assessed.

A first important result of the present study concerns the diagnostic cloud scheme. It is expected not to perform as well as the prognostic scheme in dynamic mode for long integrations, but in static mode the comparison between model and observations was not qualitatively sensitive to whether the diagnostic model or the reference prognostic cloud scheme is used. Both explain a significant portion of the observation variance, except, for both, in the Tropics at 11 μm. The diagnostic scheme explains a slightly lower portion of the variance, but has smaller biases due to different tuning. Further, the two schemes should have similar sensitivities, since one of them is a simplified version of the other one (this aspect will be documented elsewhere). As a consequence, it seems that the diagnostic model could be used in the 4D-Var observation operator in lieu of the prognostic model, which would avoid the introduction of cloud variables in the 4D-Var control vector.

Secondly, it is clear that the channels that are the most impacted by clouds are very non-linear for perturbations of the order of the current background errors in global NWP. They cannot be processed directly within the current ECMWF 4D-Var system, where only weak non-linearities are tolerated. In addition large errors were shown for these channels, both in terms of bias (which could be removed) and of standard deviations. They can be pre-processed by a local non-linear retrieval method, as is done for the geostationary atmospheric motion vectors (e.g. Schmetz et al. 1993) or in the "1D-Var+4D-Var" approach defined by Marécal and Mahfouf (2002) for rain assimilation.

In contrast, the observation operator showed much more linear and accurate behaviour for some of the upper tropospheric channels, at 4.5, 6.3 and 14.3 μm. For instance, 42 AIRS channels among the subset of 324 are selected from the following three quantitative criteria: the cloud impact on the brightness temperature (estimated from the model simulations) must be more than 0.5 K on an average, the correlations between linear and non-linear increments must exceed 0.85 (from Figure 6), and the standard deviations of the differences between diagnosed and observed brightness temperatures (computed from the numbers in Figures 3 and 4 and simply assuming uncorrelation between each other) must be below 6 K. Among the 42, 13

channels are located about 14.3 μm, 22 channels are located about 6.3 μm and 7 channels are located about 4.5 μm. At 6.3 μm water vapour absorption impedes cloud absorption and accurate linear channels can be found with lower weighting functions (i.e. which peak as low as about 400 hPa) than at 4.5 and 14.3 μm.

It is worth emphasising two features of the approach. First, accuracy is achieved in these channels despite a lower spatial resolution compared to the observations, which seems to indicate that the representativeness error is not a significant issue here. Second, the focus is on temperature and humidity fields and not on cloud variables, since the latter are diagnosed from the former. An obvious advantage is that temperature and humidity analysis increments are likely to improve the forecast far away from the analysis (e.g. Marécal and Mahfouf 2002). On the other hand, the accuracy of the present observation operator is still limited and only part of the information of the observations can be extracted. A forthcoming paper will document the available information content.

The conclusion of our assessment is that there is a potential benefit in assimilating cloud-affected satellite radiances in those spectral bands, for instance the 6.3 μm channel on-board all the geostationary satellites, *directly in 4D-Var*. This would avoid blending 4D-Var and local retrieval methods to exploit these channels in the presence of cirriform clouds. Scientific developments to the current 4D-Var systems may still be needed, for instance to improve the estimation of background error statistics, or to harmonize the resolution of the observations and the variable model resolutions within the incremental formulation. This is a concern for all types of assimilated observations.

A similar study will be performed for a selection of microwave channels in the presence of clouds and rain (Moreau et al. 2003). Channels in strong water vapour absorption bands, for instance at 22.235 GHz or 183.31 GHz, are well modelled (Chevallier and Bauer 2003) and may be sufficiently linear for direct 3D- or 4D-Var assimilation.

Acknowledgements

M. Doutriaux-Boucher at EUMETSAT coordinated the set-up of the Radiance Data from Clouds product. The kind help from P. Watts and A. McNally (ECMWF) in dealing with the AIRS data was very much appreciated. Comments from E. Andersson, A. Hollingsworth, A. Simmons and J.-N. Thépaut helped to improve the discussion.

References

Chevallier, F., P. Bauer, G. Kelly, C. Jakob, and T. McNally, 2001: Model clouds over oceans as seen from space: Comparison with HIRS/2 and MSU radiances. *J. Climate*, **14**, 4216–4229.

Chevallier, F., and G. Kelly, 2002: Model clouds as seen from space: comparison with geostationary imagery in the 11 μm channel. *Mon. Wea. Rev.*, **130**, 712–722.

Chevallier, F., P. Bauer, J.-F. Mahfouf and J.-J. Morcrette, 2002: Variational retrieval of cloud profile from ATOVS observations. *Q. J. R. Meteor. Soc.,* **128***, 2511-2526.*

Chevallier, F., and P. Bauer, 2003: Model rain and clouds over oceans: comparison with SSM/I observations. *Mon. Wea. Rev., 131, 1240-1255.*

Courtier, P., J.-N. Thépaut, and A. Hollingsworth, 1994: A strategy for operational implementation of 4D-Var, using an incremental approach. *Q. J. Roy. Meteor. Soc.*, **120**, 1367-1388.

Dee, D. P., and A. M. da Silva, 2003: The choice of variable for atmospheric moisture analysis. *Mon. Wea. Rev.*, **131**, 155-171.

Derber, J. and F. Bouttier, 1999: A reformulation of the background error covariance in the ECMWF global data assimilation system. *Tellus*, **40A**, 1-25.

Eyre, J. R., 1991: A fast radiative transfer model for satellite sounding systems. *ECMWF Technical Memorandum No. 176*, 28 pp.

Harris, B. A., and G. Kelly, 2001: A Satellite Radiance Bias Correction Scheme for Radiance Assimiliation. *Q. J. Roy. Meteor. Soc.*, **127**, 1453-1468.

Ide, K., P. Courtier, M. Ghil, and A. Lorenc, 1997: Unified notation for data assimilation: Operational, sequential and variational. *J. Met. Soc. Japan*, **75**, 181-189.

Janisková, M., J.-F. Mahfouf, J.-J. Morcrette, and F. Chevallier, 2002: Linearized radiation and cloud schemes in the ECMWF model: development and evaluation. *Q. J. R. Meteor. Soc.,* **128***, 1505-1528.*

Lorenc, A. C. and coauthors, 2000: The Met. Office global three-dimensional variational data assimilation scheme. *Q. J. R. Meteor. Soc.,* **126***, 2991-3012.*

Marécal, V., and J.-F. Mahfouf, 2002: Four dimensional variational assimilation of total column water vapor in rainy areas. *Mon. Wea. Rev.*, **130**, 43–58.

McNally, A. P. 2002: A note on the occurence of cloud in meteorologically sensitive areas and the implications for advanced infrared sounders. *Q. J. Roy. Meteor. Soc.*, **585**, 2551-2556.

McNally, A. P. and P. D. Watts, 2003: A cloud detection algorithm for high spectral resolution infrared sounders. *Q. J. Roy. Meteor. Soc.*, in press.

Moreau, E., P. Bauer, and F. Chevallier, 2003: Variational retrieval of rain profiles from spaceborne passive microwave radiance observations. *J. Geophys. Res.*, in press.

Moreau, E., P. Lopez, P. Bauer, A. M. Tompkins, M. Janisková, and F. Chevallier, 2003: Variational retrieval of temperature and humidity profiles using rain rates versus microwave brightness temperatures. ECMWF Tech. Memo. No. 412

Munro, R., G. Kelly, and R. Saunders, 1999: Assimilation of Meteosat Radiance Data within the 4DVAR System at ECMWF. Programme Report, 41 pp.

Rabier, F., A. McNally, E. Andersson, P. Courtier, P. Undén, J. Eyre, A. Hollingsworth and F. Bouttier, 1998 : The ECMWF implementation of three dimensional variational assimilation (3D-Var). Part II : Structure functions. *Q. J. Roy. Meteor. Soc.*, **124**, 1809-1829.

Rabier, F., H. Järvinen, E. Klinker, J.-F. Mahfouf and A. Simmons, 2000: The ECMWF operational implementation of four dimensional variational assimilation. Part I : Experimental results with simplified physics. *Q. J. Roy. Meteor. Soc.*, 1143-1170.

Räisänen, P., 1998: Effective longwave cloud fraction and maximum-random overlap clouds - a problem and a solution. *Mon. Wea. Rev.*, **126**, 3336-3340.

Saunders, R. W., P. Brunel, F. Chevallier, G. Deblonde, S. J. English, M. Matricardi, P. J. Rayer, 2002: RTTOV-7 - Science and validation report. *Forecasting Research Technical Report No. 387, 51 pp.* [available from the Met Office London Road, Bracknell RG12 2SZ, UK]

Schmetz, J. and O. Turpenheim, 1988: Estimation of the upper-tropospheric relative humidity field from METEOSAT water vapor image data. *J. Appl. Meteor.,* **27***, 889-899.*

Schmetz, J., K. Holmlund, J. Hoffman, B. Strauss, B. Mason, V. Gaertner, A. Koch and L. Van De Berg, 1993: operational cloud-motion winds from Meteosat infrared images. *J. Appl. Meteor.,* **32***, 1206-1225.*

Simpson, J. and V. Wiggert, 1969: Models of precipitating cumulus towers. *Mon. Weather Rev.*, 97,471-489.

Stokes, G. M., and S. E. Schwartz, 1994: The Atmospheric Radiation Measurement (ARM) Program: programmatic background and design of the cloud and radiation testbed. *Bull. Amer. Meteo. Soc.*, **75**, 1201-1221.

Tiedtke, M., 1989: A comprehensive massflux scheme for cumulus parametrization in large-scale models. *Mon. Wea. rev.*, **117**, 1779-1800.

Tiedtke, M., 1993: Representation of clouds in large-scale models. *Mon. Wea. rev.*, **121**, 3040-3061.

Tompkins, A. M. and M. Janisková, 2003: A cloud scheme for data assimilation: description and initial tests. ECMWF Tech. Memo. No. 410

MVIRI channel	O		D - P		D- O		P - O	
	Mean	Std.	Mean	Std.	Mean	Std.	Mean	Std.
6.3 μm	234.1	7.9	0.2	2.6	1.3	5.8	1.2	5.7
11 μm	260.9	18.4	-1.5	9.6	8.2	18.0	9.7	16.5

Table 1: Mean and standard deviation of the observations (O) and of the differences between the two model brightness temperatures or between modelled and observed brightness temperatures, in degrees Kelvin. The model cloud variables are either prognosticated (P) or diagnosed (D). Statistics are presented for the two MVIRI infrared channels and are restricted to the Meteosat quadrants where less than 70% of the pixels are judged clear (10770 quadrants out of 22718).

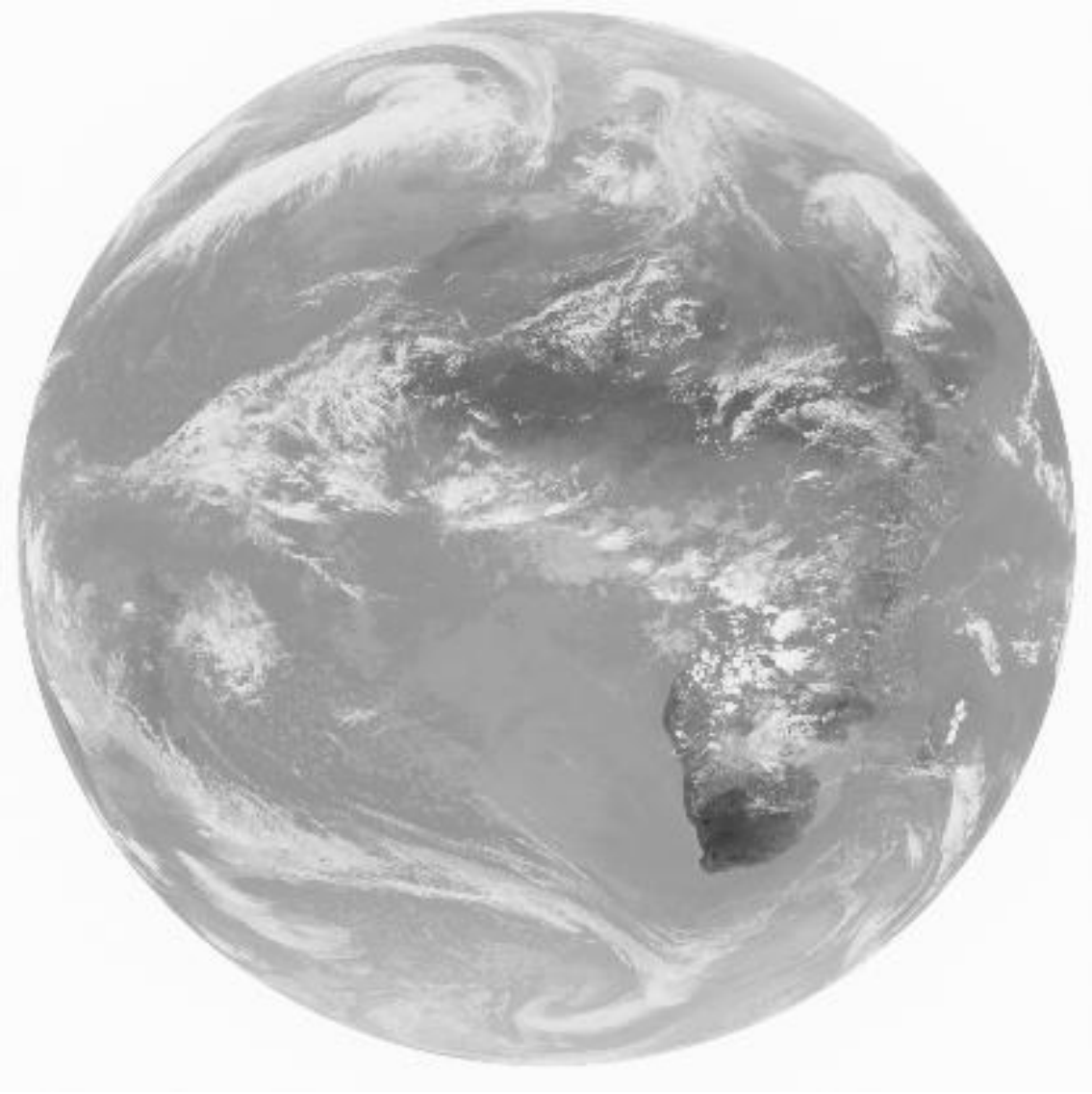

Figure 1: Observed Meteosat-7 11 μm image on 30 November 2002 at 12 UTC.

(a) 6.3 μm

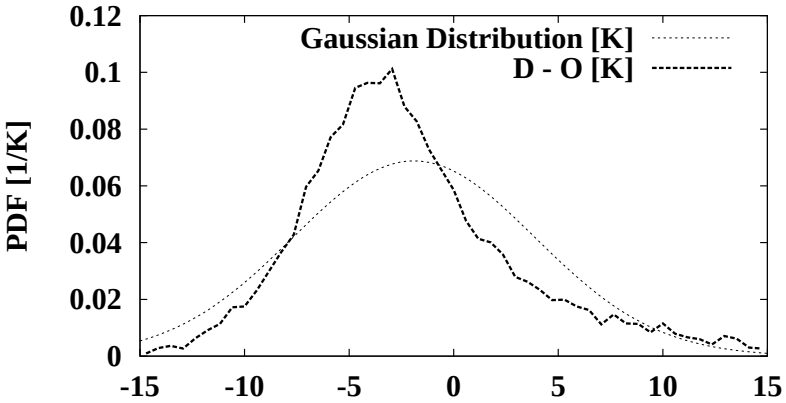

(b) 11 μm

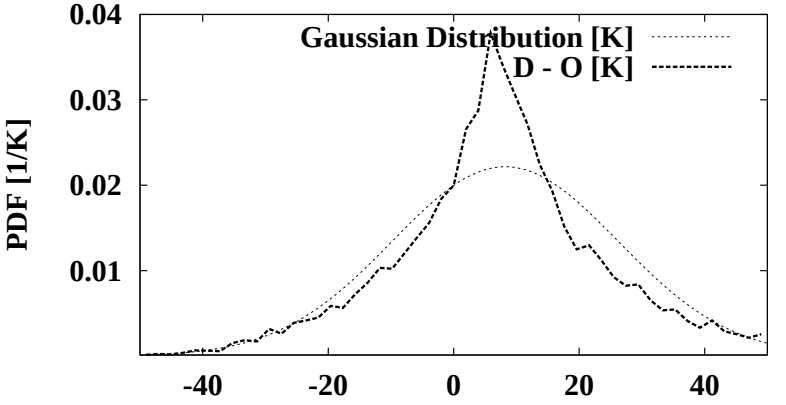

Figure 2: Probability density function (PDF) of the departures between diagnostic-model (D) and observed (O) MVIRI 6.3 and 11 μm brightness temperatures in the Meteosat-7 cloudy quadrants of 30 November 2002 at 12 UTC. The Gaussian distributions with the same means and standard deviations are also reported on the graphs.

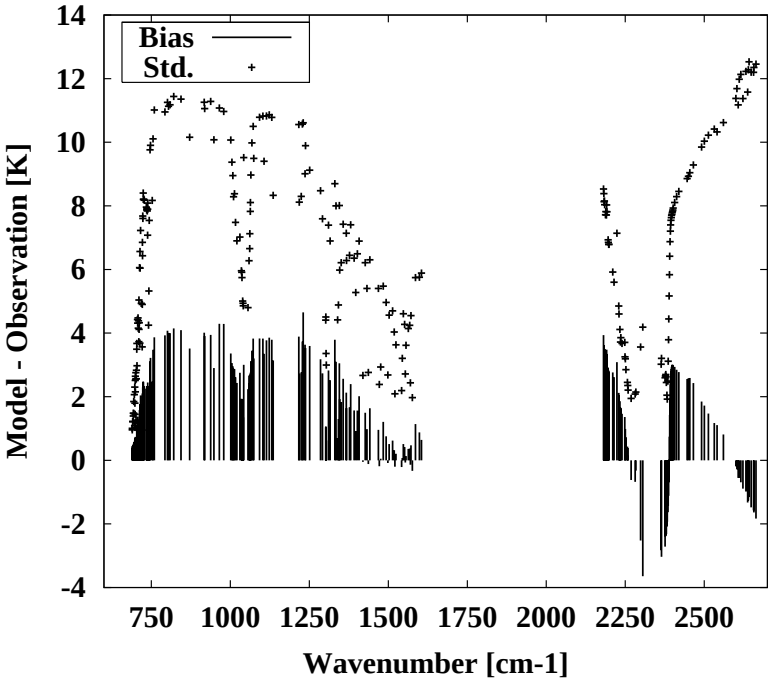

Figure 3: Bias and standard deviation of the differences between the model and the cloud-affected observed AIRS brightness temperatures on 30 November 2002. The model uses the prognostic cloud scheme. Above 2000 cm^{-1} day-time pixels are discarded. For comparison, the filter functions of the infrared MVIRI channel cover wavenumbers between 1351 and 1818 cm^{-1} around 6.3 μm and those between 770 and 976 cm^{-1} around 11 μm.

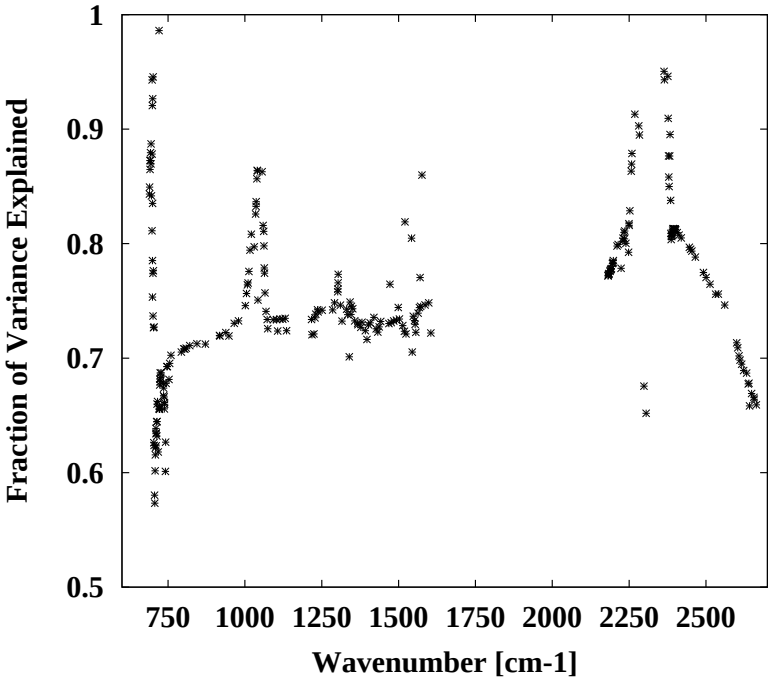

Figure 4: Fraction of observation variance explained by the model for the cloud-affected AIRS data on 30 November 2002. The model uses the prognostic cloud scheme.

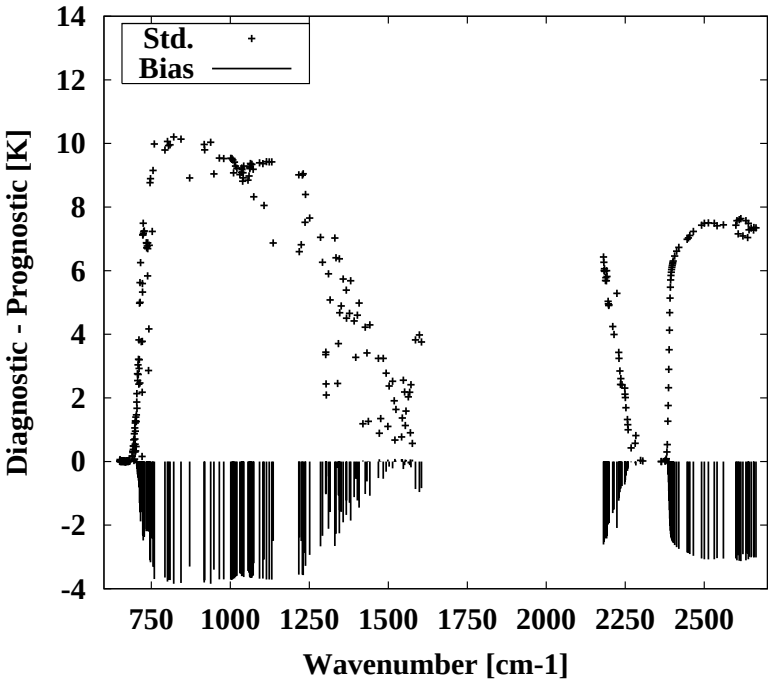

Figure 5: Bias and standard deviation of the differences between the model diagnostic and prognostic AIRS brightness temperatures. Model data correspond the Meteosat-7 disk on 30 November 2002 at 12 UTC. Clear points are removed using the Meteosat-7 cloud detection. In contrast to Figure 3, stratospheric channels are not removed.

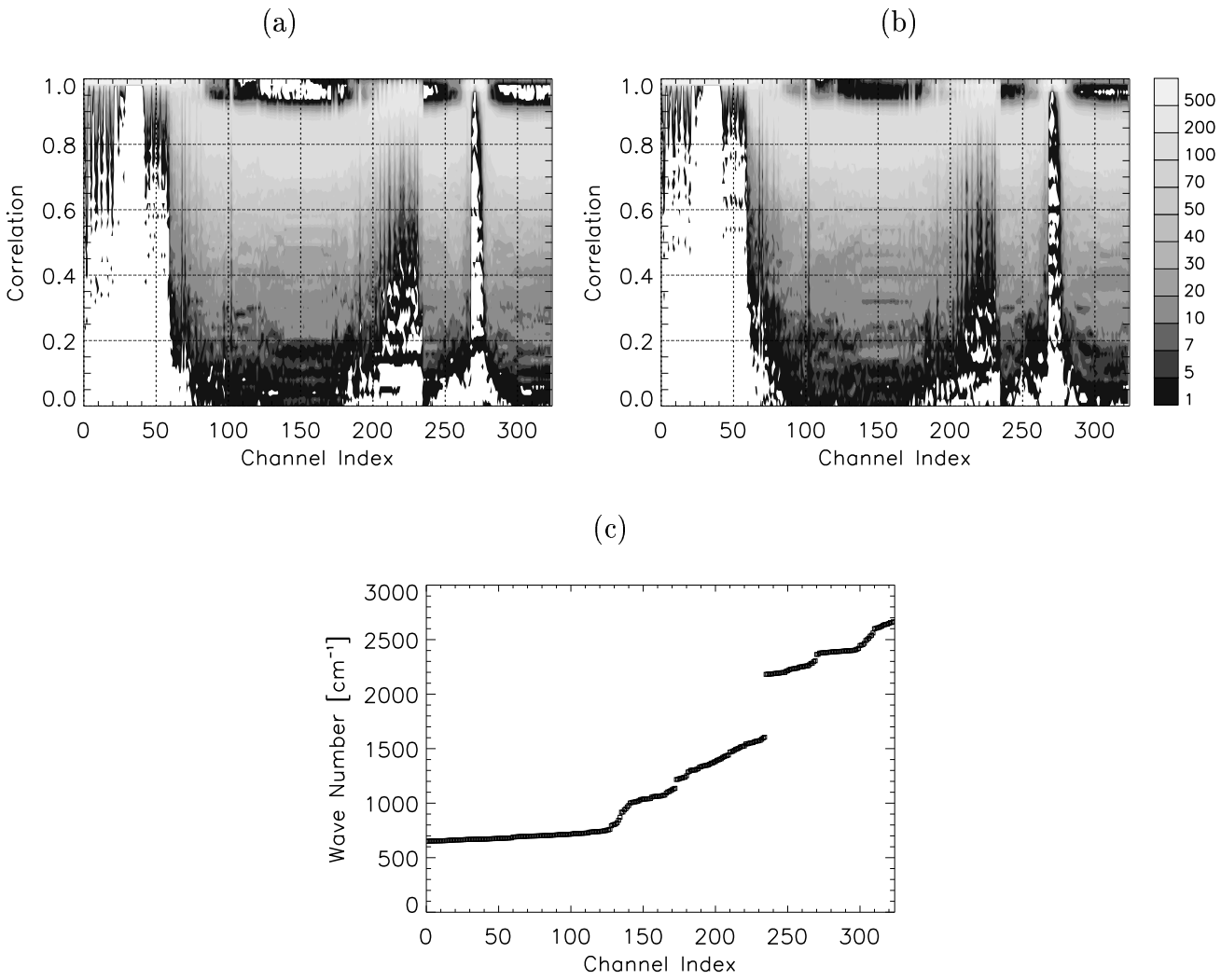

Figure 6: Figures (a) and (b) present bi-dimensional histograms of the correlation between linear and non-linear brightness temperature perturbations for each one of the 324 AIRS channel subset. The input temperature and humidity perturbations follow the statistics of the ECMWF background error in Figure (a). Temperature perturbations are the same in Figure (b), but humidity ones are divided by two. Negative correlations are not represented. The colour code for the number of items represented in the histogram bins appears next to Figure (b). The correspondence between channel index and wave number is shown in Figure (c).